Ab-initio study of germanium *di*−interstitial using a hybrid functional (HSE)

E. Igumbor[a,b,*], C. N. M. Ouma[a], G. Webb[a], W. E. Meyer[a,**]

[a]*Department of Physics, University of Pretoria, Pretoria 0002, South Africa.*
[b]*Department of Mathematics and Physical Sciences, Samuel Adegboyega University, Km 1 Ogwa/Ehor Rd, Ogwa Edo State Nigeria.*

Abstract

In this work, we present *ab-initio* calculation results of Ge *di*−interstitials ($I_{2(Ge)}$) in the framework of the density functional theory (DFT) using the Heyd, Scuseria, and Ernzerhof (HSE) hybrid functional. The formation energy, transition levels and minimum energy configurations were obtained for $I_{2(Ge)}$ −2, −1, 0, +1 and +2 charge states. The calculated formation energies shows that for all charge states of $I_{2(Ge)}$, the double tetrahedral (T) configuration formed the most stable defect with a binding energy of 1.24 eV in the neutral state. We found the (+2/+1) charge state transition level for the T lying below the conduction band minimum and (+2/+1) for the split[110]-tetrahedral configuration lying deep at 0.41 eV above the valence band maximum. The *di*-interstitials in Ge exhibited the properties of both shallow and deep donor levels at (+2/+1) within the band gap and depending on the configurations. $I_{2(Ge)}$ gave rise to *negative-U*, with *effective-U* values

*Corresponding author
**Corresponding author
Email addresses: elgumuk@gmail.com (E. Igumbor), wmeyer@up.ac.za (W. E. Meyer)

Preprint submitted to Physica B *November 30, 2015*

of -0.61 and -1.6 eV in different configurations. We have compared our results with calculations of *di*-interstitials in silicon and available experimental data.
Keywords: interstitial, defects, charge state

---

1. Introduction

The application of germanium (Ge) as a promising material for complementary metal-oxide semiconductors (CMOS) technology is attracting attention due to its narrow band gap, high carrier mobility and low voltage operations[1, 2]. For successful technology, industrial application and utilization of Ge based devices, it should be single crystalline and free of detrimental defects. The knowledge of formation and transition charge state energies are of interest in defects, and the understanding of defects and their transition charge state energies within the band gap are important towards controlling and engineering their formation in order to improve the material quality. Based on the charge states properties of defects in Ge, it is possible to understand the characteristics of electron irradiation damage and its dependency on the Fermi level. Progress in the identification of electron irradiation damage defects was interrupted by investigations into radiation defects in Silicon (Si), but has now become topical again owing to the higher carrier mobilities realized in Ge based devices [3]. Defect studies in Ge are not too common, particularly those dealing with the atomic and electronic details of elemental radiation induced defects. This deficiency does not only apply to experimentation [4] but to modeling as well [5]. Recently, deep level transient spectroscopy (DLTS) [6, 7] and infrared absorption spectroscopy [4]

studies have succeeded in identifying new radiation defects paired with impurities. Perturbed angular correlation spectroscopy (PACS) studies [8] have led to important findings on the mobility and electrical activity of vacancies (V) and interstitials (I); these two defects created following low temperature radiation, have been investigated by in situ DLTS [7, 8].

Various theoretical investigations have attempted to explain experimental data [9, 7, 10], where some progress has been achieved in understanding the properties of vacancy, *self*- and interstitial related defects in Ge. In a detailed study of interstitial and vacancies in Ge using local density approximation (LDA) and generalized gradient approximation (GGA) [11], the energetic, stability and equilibrium of different configurations were investigated, and interstitials in Ge were found to be bistable having a double donor when at cage site, without any trace of acceptor [12]. The split[110] interstitial has been reported to be more energetically stable than the tetrahedral and hexagonal configurations [9]. The split[110] interstitial configurations were reported to have an acceptor level located at $E_V + 0.45$ eV, while the tetrahedral acts as a donor at $E_V + 0.11$ eV and $E_V + 0.46$ eV for the (+2/+1) and (0/+1) occupancy levels [9, 13] respectively. According to Janke *et al* [14] vacancy defects in Ge will anneal by diffusion provided the trap density is high enough. *Self*-interstitial reflection by Ge surfaces has been proposed [15] to explain the results of diffusion experiments during irradiation. This analysis was extended to diluted SiGe alloys, which provides some explanation of the theoretical donor level calculations for pure Si and alloys with a different Ge content [16]. Cowern *et al* [17] reported Ge to be a complex, mutable with a structure similar to an amorphous pocket. Analogous morph structures are

expected to exist for both the $self$-interstitial and the vacancy in Si. This paved the way for the study of trivacancy, trivacancy-oxygen complexes and $self$-interstitial clusters in Si and Ge. Defect studies of Si in particular, *self-, di-, tri-* and *small cluster* interstitials [18, 19] and vacancies [20, 21] have been reported. However contrary to Si no *di-* and *small cluster* interstitials of intrinsic defects in Ge have been accomplished, thus a detailed formation energy, transition charge states calculation and interpretation of results of *di*-interstitial are still missing. In this work we have carried out hybrid functional of Heyd, Scuseria, and Ernzerhof (HSE) [22, 23] calculations of $I_{2(Ge)}$ in the double split[110] (SP10), split[110]-tetrahedral (SPT) and double tetrahedral (T) configurations. We calculated the formation and transition charge state energies within the band gap as was reported in the case of Si [18, 12] with a view to finding the most energetically stable configuration, and finally compared our results with experimental and other available data.

2. Computational details

DFT electronic structure calculations were performed in the Vienna $ab-$ *initio* Simulation Package (VASP) [24, 25]. We used projector-augmented wave (PAW), as implemented in the VASP code to separate the inert core electrons from the chemically active valence electrons [25, 26, 27]. Calculations were carried out using the Heyd, Scuseria, and Ernzerhof (HSE) [22, 23] hybrid functional. In this approach, the short-range exchange potential is calculated by mixing a fraction of nonlocal Hartree-Fock exchange with the generalized gradient approximation (GGA) functional of Perdew, Burke, and Ernzerhof (PBE) [11]. The hybrid functional introduces a percentage of ex-

act non-local Fock exchange (25%) to the PBE functional [22, 23]. For the bulk, geometric optimization of Ge was performed in the primitive unit cell by means of the 8^3 Monkhorst-Pack [28] k-points Brillouin zone sampling scheme and cutoff energy of 400 eV. Relaxations converged when the forces on all the atoms were less than 0.01 eV/Å. For the pure Ge, we employed 64 atom supercells, and for the defects, two Ge atoms were introduced into the 64 supercell atoms. We then used the 2^3 Monkhorst-Pack [28] special k-points Brillouin zone sampling scheme, achieving convergence of the total energy by setting the energy cutoff of the wave function expansion for the charge states to 600 eV. Spin orbit coupling was taken into account in all the calculations. The *concentrations* (C) of defects in thermodynamic equilibrium are related to the formation energy (E^f) through Boltzmann constant

$$C = N_0 \exp(-E^f/k_B T), \quad (1)$$

where $k_B T$ is the temperature in eV and N_0 the number of possible defects sites. In Eq. 1 the increase in formation energies leads to decrease in the concentration of the defects. For the defect charge states, E^f depends on Fermi level (ε_F). E^f of defects are derived directly from total energies, allowing the calculation of equilibrium defect *concentrations* [29]. To calculate the defects E^f and transition energy ($\epsilon(q/q')$) levels, we calculated the total energy $E(d,q)$ for a supercell containing the optimized defect d in its charge state q. The defect formation energy $E^f(d,q)$ as a function of electron Fermi energy (ε_F) is given as [29, 30]

$$E^f(d,q) = E(d,q) - E(pure) + \sum_i \triangle(n)_i \mu_{Ge} + q[E_V + \varepsilon_F + \triangle V] + \triangle^q, \quad (2)$$

where $E(pure)$ is a supercell without a defect, $\triangle(n)_i$ is the difference in the number of constituent atoms of type i between the supercells, E_V is the valence band maximum (VBM) and μ_{Ge} =−5.18 eV is the chemical potential of germanium. For us to pay special attention to the uncertainties surrounding the calculation of $E^f(d,q)$ due to finite-size effects within the supercell and inaccuracy underlying the approximation of energy functional, we have included the electrostatic alignment $\triangle V$ and the image charge correction ($\triangle^q$) according to Freysoldt *et al* [31, 32]. The defect transition energy level $\epsilon(q/q')$ is the Fermi energy for which the formation energy of charge state q equals that of charge state q' is given as [30]

$$\epsilon(q/q') = \frac{E^f(d,q;\ \varepsilon_F = 0) - E^f(d,q';\ \varepsilon_F = 0)}{q' - q} \tag{3}$$

The method proposed by Stephan *et al* [33] was taken into account for the calculation of the ionization energy (I_A) with reference to the conduction band (CBM) and the electron affinity (E_A) with reference to valence band maximum (VBM). The binding energy E_b which is defined as the energy required to split up an interstitial cluster into well separated non-interacting *mono*-interstitials was calculated using the method proposed by Zollo *et al* [34].

3. Results and discussion

In contrast to the LDA and GGA that underestimate the band gap of the semiconductor [13], the HSE functional gives an excellent description of the electronic band gap and charge state transition properties for a wide range of the defects in group−IV semiconductors [35]. The pristine Kohn-Sham band gap of Ge was calculated to be 0.80 eV, which was higher than the

experimental band gap at 0 K. To address the band gap problem in order to obtain the experimental band gap of Ge, we employed the quasiparticle band gap [36, 33] calculation, which from the calculated I_A and the E_A energies of 4.00 and 3.22 eV respectively, resulted in an improved Ge band gap of 0.78 eV, that is in agreement with the experimental band gap reported by Morin *et al* [37] at 0 K. For us to calculate the formation energy of $I_{2(Ge)}$, we first calculated the formation energies of Ge *self*-interstitial. For both the tetrahedral and split[110] configurations in the neutral state for *self*-interstitial, we have calculated 3.88 and 3.80 eV respective formation energies, and our results were in close agreement with earlier results [12, 13, 38] based on LDA and GGA functionals.

3.1. Structural properties and energetics of $I_{2(Ge)}$

We calculated the relaxed configurations for a number of different geometric configurations and found three competing geometric structures: split [110]-tetrahedral (SPT), split-split [110] (SP10) and tetrahedral-tetrahedral (T). These structural equilibrium configurations were obtained by adding a tetrahedral or split[110] interstitial atom to a cell containing a fully relaxed split[110] or tetrahedral single interstitial atom. The optimized structures as in the case of Si [39, 21] demonstrated that each interstitial atom of the pair forms bonds with neighboring atoms resulting in full four-fold coordination as seen in Fig. 1. Fig. 1a shows the relaxed structure of the T configuration and Fig. 1b represents the optimized structure of the SP10 configuration. This structure is obtained by combining two interstitials in the split[110], which many believe to be the most stable interstitial configuration of Ge as well as Si and in the case of Si is responsible for extremely fast migration.

Fig 1c represents the optimized structure of the SPT configuration. The defect caused a reduction in bond length as neighboring atoms and defect atoms repositioned to a position of equilibrium, the reduction being approximately between $0.02 - 0.07$Å in all the configurations. The bond angle between one of the defects and its two nearest neighbors after optimization were 110.62^0 and 113.5^0 for T and SP10 respectively. For the SPT configurations, the angles were 101^0 and 110.62^0 for the two interstitials atoms.

3.2. Electronic structure of the $I_{2(Ge)}$

The most stable structures of the $I_{2(Ge)}$ configuration were represented in Fig. 1; the formation and binding energies for the charge states are shown in Table 1. In all the configurations, the T configuration was the most stable in the neutral state. For the neutral state of $I_{2(Si)}$, the E^f of SP10 was found by Posselt *et al* [40] to be lower than that of the T configuration by 0.04 eV. Jones *et al* [21] found that the SPT configuration had an even lower formation energy. The results listed in Table 1, show positive binding energies for all configurations investigated. This agrees with results for Si obtained by Posselt *et al* [40] and Bongiorno *et al* [41], who also found positive binding energies in the SP10, T and SPT of $I_{2(Si)}$. It should be noted that, in contrast to Si, the most stable configuration for $I_{2(Ge)}$ was the T configuration. It is also interesting to know that for Ge, the SP10 configuration has a formation energy of 0.82 eV more than the T configuration while in Si the SP10 formation energy was 0.04 eV less than the T configuration formation energy.

Fig. 2 shows the formation energy of the $I_{2(Ge)}$ as a function of the Fermi-level for the different configurations. As shown in Fig. 2a and Fig. 2b, our

calculation demonstrates that $I_{2(Ge)}$ was stable in the T and SP10 configurations as a double ionized state. The energy levels of (+2/+1) and (+1/−1) transition charge states of Ge and Si were tabulated in Table 2, we have decided to limit the charge state transition levels of $I_{2(Si)}$ to (+1/−1) and (+2/+1) since other levels were not present in our calculation. For the T configuration, the (+2/+1) level lies above the valence band, with a value of 0.74 eV referencing the VBM. The SP10-configuration transition state level for (+2/+1) was 0.41 eV which was lying deep, almost in the middle of the band gap. The (+2/+1) donor level found in both the T and SP10 configurations exhibit both shallow and deep levels respectively. Donor level property was not only found in *di*-interstitial but also in self-interstitial for the T configuration at $E_C - 0.06$ eV. For the SPT configuration, as represented in Fig. 2c there was no transition state level found within the band for (+2/+1). Instead we found a deep lying level of (+1/−1), which was not the case for the Si in SP10 configuration where it was earlier found that the (+2/+1) shallow level was 0.03 eV lying close to the valence band [21]. The behavior of +1 and +2 charge state of $I_{2(Si)}$ is tied to the valence band where as in Ge it is close to the conduction band for the T and deep in the band gap for the SP10 configuration. Since $I_{2(Ge)}$ defects transition state levels were positively charged (+1 and +2), they should exhibit a poole-Frenkel effect (field assisted thermal ionization): which occurs as a result of the lowering of a coulombic potential barrier when it interacts with the field in the presence of a positively charged trap which gives rise to interaction between the positively charged trap and the electron [42]. Information on the relative stability of different charge states for a specific defect are contained in the

formation energy. The charge-state transition levels $\epsilon(q/q')$, delineate the energy regions over which particular charge states are stable. The normal arrangement is $\epsilon(+1/0) < \epsilon(0/-1)$ indicating a positive repulsive energy U when electrons are added. However we sometimes witness ordering, of this type $\epsilon(0/-1) < \epsilon(+1/0)$, a term that is referred to *negative*$-U$. It is interesting to know that while Si shows traces of acceptor on the contrary we discovered that Ge exhibits properties of *negative-*U in the SPT and SP10 configurations. Fig. 2b and Fig. 2c, clearly show the $(+1/-1)$ transition level at $E_V + 0.47$ and $E_V + 0.58$ eV in SPT and SP10 configurations respectively. The *effective-*U arising from this large difference of lattice relaxation for SPT and SP10 configurations was -0.61 and -1.6 eV respectively. Both the *di*-interstitial and *self*-interstitial of Ge did not show any acceptor-like level in any configuration, and negative charge states were never the most stable in our calculation; which is in contrast to the $(0/-1)$ transition state level found in $I_{2(Si)}$ [19]. No metastability was predicted in any configuration of $I_{2(Ge)}$, whereas Lee *et al* [43] predicted metastability for the $I_{2(Si)}$. The electronic energy calculation has shown that the $I_{2(Ge)}$ is more stable than the *mono*-interstitial, and that it existence can be examined by exploring shallow donors near the conduction band edge.

4. Conclusion

In summary we have carried out detailed calculations of $I_{2(Ge)}$ defects in different configurations, using the Heyd, Scuseria, and Ernzerhof (HSE) hybrid functional in the framework of DFT. The electronic and structural properties of these configurations were described in detail. We have shown

that the formation of $I_{2(Ge)}$ from two neutral isolated interstitials was energetically favourable. Our calculation shows that the tetrahedral (T) configuration, where both interstitials were at a tetrahedral site, was more stable than the split[110]-tetrahedral (SPT) and double split[110] (SP10) configurations by more than 0.8 eV, therefore the T configuration should dominate under equilibrium conditions. In this configuration, *di*-interstitials exhibit the property of a shallow donor (+2/+1) at $E_C - 0.04$. In the SP10, deep levels at $E_V + 0.41$ eV for (+2/+1) and $E_V + 0.47$ for (+1/−1) were predicted, while in SPT only a deep level at $E_V + 0.58$ eV for (+1/−1) was predicted. We observed the presence of *negative-U* having *effective-U* values of −0.61 and −1.6 eV for the SPT and SP10 configurations respectively. We pointed out the role of $I_{2(Ge)}$ in an electrically activating donor. We expect the data presented to be useful in the process modeling of Ge-based devices.

5. Acknowledgement

This work is based on the research supported partly by National Research foundation (NRF) of South Africa (Grant specific unique reference number (UID) 78838). The opinions, findings and conclusion expressed are those of the authors and the NRF accepts no liability whatsoever in this regards.

[1] C. Chui, H. Kim, P. McIntyre, K. Saraswat, Technical Digest - International Electron Devices Meeting (2003) 437–440.

[2] M. Houssa, A. Satta, E. Simoen, B. De, M. Jaeger, M. Caymax, M. Heyns, Germanium-Based Technologies: From Materials to Devices (2011) 233.

[3] L. Lee, E. A. Fitzgerald, T. Bulsara, Mayank, T. Currie, A. Lochtefeld, Journal of Applied Physics 97 (1) (2005) 011101.

[4] J. Fage-Pedersen, A. N. Larsen, A. Mesli, Phys. Rev. B 62 (2000) 10116–10125.

[5] J. Coutinho, R. Jones, P. R. Briddon, S. Öberg, Phys. Rev. B 62 (2000) 10824–10840.

[6] V. P. Markevich, I. D. Hawkins, A. R. Peaker, V. V. Litvinov, L. I. Murin, L. Dobaczewski, J. L. Lindstrm, Applied Physics Letters 81 (10) (2002) 1821–1823.

[7] F. D. Auret, S. M. M. Coelho, M. Hayes, W. E. Meyer, J. M. Nel, physica status solidi (a) 205 (1) (2008) 159–161.

[8] H. Haesslein, R. Sielemann, C. Zistl, Phys. Rev. Lett. 80 (1998) 2626–2629.

[9] M. D. Moreira, R. H. Miwa, P. Venezuela, Phys. Rev. B 70 (2004) 115215.

[10] A. Giese, N. A. Stolwijk, H. Bracht, Applied Physics Letters 77 (5) (2000) 642–644.

[11] J. P. Perdew, K. Burke, M. Ernzerhof, Phys. Rev. Lett. 77 (1996) 3865–3868.

[12] A. Carvalho, R. Jones, C. Janke, J. P. Goss, P. R. Briddon, J. Coutinho, S. Öberg, Phys. Rev. Lett. 99 (2007) 175502.

[13] P. Śpiewak, J. Vanhellemont, K. Sueoka, K. Kurzydłowski, I. Romandic, Materials Science in Semiconductor Processing 11 (5) (2008) 328–331.

[14] C. Janke, R. Jones, S. Öberg, P. R. Briddon, Phys. Rev. B 75 (2007) 195–208.

[15] E. Kamiyama, K. Sueoka, J. Vanhellemont, Journal of Applied Physics 113 (9) (2013) 5.

[16] J. P. Leitão, A. Carvalho, J. Coutinho, R. N. Pereira, N. M. Santos, A. O. Ankiewicz, N. A. Sobotitlev, M. Barroso, J. Lundsgaard Hansen, A. Nylandsted Larsen, P. R. Briddon, Phys. Rev. B 84 (2011) 165211.

[17] N. E. B. Cowern, S. Simdyankin, C. Ahn, N. S. Bennett, J. P. Goss, J.-M. Hartmann, A. Pakfar, S. Hamm, J. Valentin, E. Napolitani, D. De Salvador, E. Bruno, S. Mirabella, Phys. Rev. Lett. 110 (2013) 155501.

[18] S. K. Estreicher, M. Gharaibeh, P. A. Fedders, P. Ordejón, Physical review letters 86 (7) (2001) 1247.

[19] G. M. Lopez, V. Fiorentini, Physical Review B 69 (15) (2004) 155206.

[20] V. P. Markevich, A. R. Peaker, S. B. Lastovskii, L. I. Murin, J. Coutinho, V. J. B. Torres, P. R. Briddon, L. Dobaczewski, E. V. Monakhov, B. G. Svensson, Phys. Rev. B 80 (2009) 235207.

[21] R. Jones, T. A. G. Eberlein, N. Pinho, B. J. Coomer, J. P. Goss, P. R. Briddon, S. Öberg, Nuclear Instruments and Methods in Physics Research 186 (1) (2002) 10–18.

[22] J. Heyd, G. E. Scuseria, M. Ernzerhof, The Journal of Chemical Physics 118 (18) (2003) 8207–8215.

[23] J. Heyd, G. E. Scuseria, M. Ernzerhof, The Journal of Chemical Physics 124 (21).

[24] G. Kresse, J. Furthmültitler, Phys. Rev. B 54 (1996) 11169–11186.

[25] G. Kresse, D. Joubert, Phys. Rev. B 59 (1999) 1758–1775.

[26] G. Kresse, J. Furthmltitler, Computational Materials Science 6 (1) (1996) 15 – 50.

[27] P. E. Blochl, Phys. Rev. B 50 (1994) 17953–17979.

[28] H. J. Monkhorst, J. D. Pack, Phys. Rev. B 13 (1976) 5188–5192.

[29] S. B. Zhang, J. E. Northrup, Phys. Rev. Lett. 67 (1991) 2339–2342.

[30] Freysoldt, Christoph, Grabowski, Blazej, Hickel, Tilmann, J. Neugebauer, Kresse, Georg, Janotti, Anderson, V. de Waltitle, C. G., Rev. Mod. Phys. 86 (2014) 253–305.

[31] C. Freysoldt, J. Neugebauer, C. G. Van de Walle, Phys. Rev. Lett. 102 (2009) 016402.

[32] C. Freysoldt, J. Neugebauer, C. G. Van de Walle, physica status solidi (b) 248 (5) (2011) 1067–1076.

[33] S. Lany, A. Zunger, Phys. Rev. B 78 (2008) 235104.

[34] G. Zollo, Y. J. Lee, R. M. Nieminen, Journal of Physics: Condensed Matter 16 (49) (2004) 8991.

[35] P. Deák, B. Aradi, T. Frauenheim, E. Janzén, A. Gali, Phys. Rev. B 81 (2010) 153203.

[36] J. P. Perdew, M. Levy, Phys. Rev. Lett. 51 (1983) 1884–1887.

[37] F. J. Morin, J. P. Maita, Phys. Rev. 94 (1954) 1525–1529.

[38] R. Jones, A. Carvalho, J. Goss, P. Briddon, Materials Science and Engineering: B 159 (2009) 112–116.

[39] T. A. G. Eberlein, N. Pinho, R. Jones, B. J. Coomer, J. P. Goss, P. R. Briddon, S. Öberg, Physica B: Condensed Matter 308 (2001) 454–457.

[40] M. Posselt, F. Gao, D. Zwicker, Phys. Rev. B 71 (2005) 245202.

[41] A. Bongiorno, L. Colombo, F. Cargnoni, C. Gatti, M. Rosati, EPL (Europhysics Letters) 50 (5) (2000) 608.

[42] J. G. Simmons, Phys. Rev. 155 (1967) 657–660.

[43] S. Lee, G. S. Hwang, Phys. Rev. B 77 (2008) 085210.

[44] D. A. Richie, J. Kim, S. A. Barr, K. R. A. Hazzard, R. Hennig, J. W. Wilkins, Phys. Rev. Lett. 92 (2004) 045501.

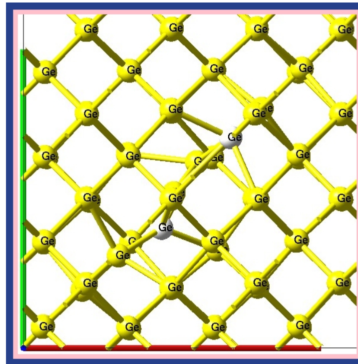

(a)

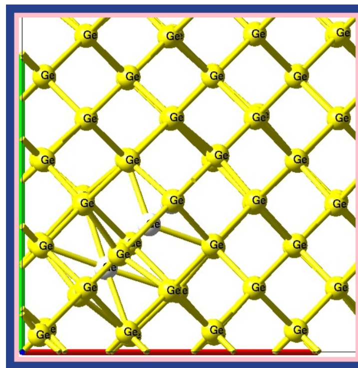

(b)

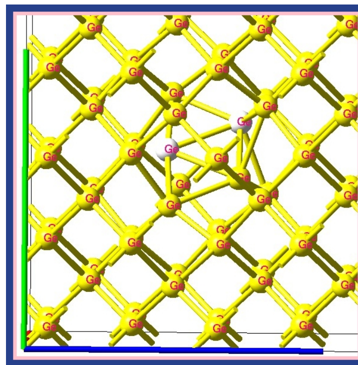

(c)

Figure 1: (a) Optimized structure of T; double tetrahedral interstitial atoms, (b) Optimized structure of SP10; double split[110] interstitial atoms and (c) Optimized structure of SPT; split[110] and tetrahedral interstitial atoms. All interstitial atoms in white for the various configurations.

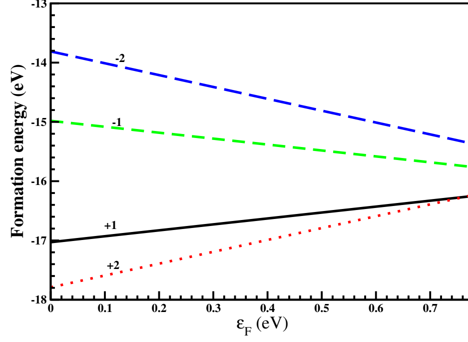

(a) T configuration

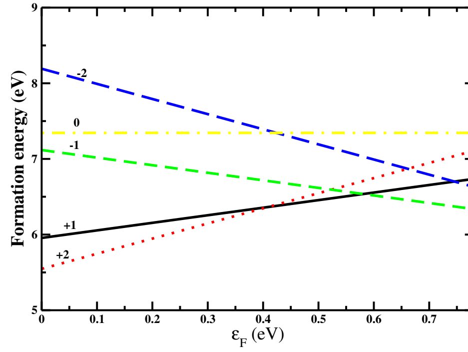

(b) SP10 configuration

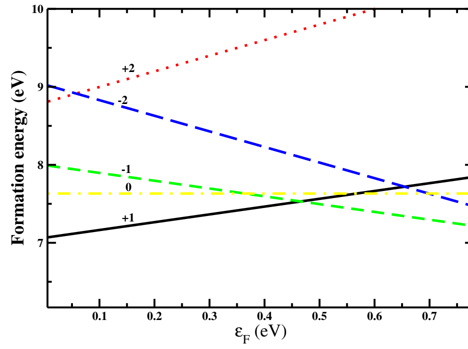

(c) SPT configuration

Figure 2: Plot of formation and Fermi energies of T, SPT and SP10 configurations of $I_{2(Ge)}$ as a function of the Fermi energy (ε_F), indicating the different charge states and transition levels observed withing the band gap. The SPT and SP10 configurations, show *negative-U* property. We have used the quasiparticle like band gap of 0.78 eV since it was in agreement with experimental band gap result at $0K$.

Table 1: Calculated formation E^f and binding energies E_b in eV for the neutral state of the various defect configurations. We have included other references for easy comparison. Our work in bold.

defects	SP10	T	SPT
Ge_i (E^f)	**3.80**	**3.88**	not applicable
	3.54 [9]	3.79 [13]	
	3.56 [13]	3.84 [9]	
$I_{2(Ge)}$ (E^f)	**7.34**	**6.52**	**7.63**
$I_{2(Si)}$ (E^f)	6.10[40]	6.14[40]	5.12 [21]
		6.46 [44]	4.91 [41]
$I_{2(Ge)}$ (E_b)	**0.26**	**1.24**	**0.05**
$I_{2(Si)}$ (E_b)	1.74[40]	1.70[40]	1.41 [41]

Table 2: Calculated transition states $(+2/+1)$ and $(+1/-1)$ levels (eV) of $I_{2(Ge)}$and $I_{2(Si)}$. This work in bold.

Defects	SP10	T	SPT
$I_{2(Ge)}$ $(+2/+1)$	**E_V + 0.41**	**E_C - 0.04**	-
$I_{2(Ge)}$ $(+1/-1)$	**E_V + 0.58**		**E_V + 0.47**
$I_{2(Si)}$ $(+2/+1)$	E_V + 0.03 [21]		E_V + 0.20 [19]